LAWRENCE
LIVERMORE
NATIONAL
LABORATORY

LLNL-JRNL-404826

Measurement of Preheat and Shock Melting in Be Ablators During the First Few ns of the NIF Ignition Pulse

D. K. Bradley, S. T. Prisbrey, R. H. Page, D. G. Braun, M. J. Edwards, R. L. Hibbard, K. A. Moreno, M. P. Mauldin, A. Nikroo

June 23, 2008

Physics of Plasmas

Disclaimer

Measurements of preheat and shock melting in Be ablators during the first few ns of the NIF ignition pulse

D. K. Bradley, S. T. Prisbrey, R. H Page, D. G. Braun, M. J. Edwards, and R. Hibbard

Lawrence Livermore National Laboratory, 7000 East Ave. Livermore CA 94550

K. A. Moreno, M. P. Mauldin, A. Nikroo

General Atomics, San Diego, CA 92186

Abstract

We have developed a scaled hohlraum platform to experimentally measure preheat in ablator materials during the first few nanoseconds of the radiation drive proposed for ignition experiments at the National Ignition Facility {J. A. Paisner, J. D. Boyes, S. A. Kumpan, *et al*., Laser Focus World **30**, 75 (1994)}. The platform design approximates the radiation environment of the pole of the capsule by matching both the laser spot intensity and illuminated hohlraum wall fraction in scaled halfraums driven by the OMEGA laser system { T. R. Boehly, D. L. Brown, R. S. Craxton, et al., Optics Communications **133**, 495 (1997)}. A VISAR reflecting from the rear surface of the sample was used to measure sample motion prior to shock breakout. The experiments show that the first ~20 μm of a Be ablator will be melted by radiation preheat, with subsequent material melted by the initial shock, in agreement with simulations. The experiments also show no evidence of anomalous heating of buried high-z doped layers in the ablator.

Introduction

Inertial confinement fusion (ICF) involves the compression of thermonuclear fuel to high densities and temperatures [1]. In order to achieve ignition a capsule, consisting of a low-Z ablator material surrounding a cryogenic layer of fusion fuel, is imploded to compress the fuel to an areal density of ~2000 mg/cm^2. In current designs for ICF using the National Ignition Facility (NIF)[2] the capsule is driven by a series of 4 increasing pressure pulses or shocks, generated by X-ray ablation of the capsule inside a high-Z radiation case, or hohlraum . The sequence of shocks is carefully tailored to maintain the fuel on a low isentrope as the implosion progresses[1]. An important factor that can limit the performance of ICF implosions is the development of hydrodynamic instabilities due to imperfections at the fuel/capsule interface. These imperfections are Rayleigh-Taylor (RT) unstable[3, 4] and can grow by factors of 100 or more during the acceleration of the fuel. Seeds for the instability can come from both surface roughness and velocity perturbations imposed on the shock waves via material inhomogenieties, such as voids, in the ablator. Growth of the instabilities at the fuel/pusher interface induces mixing of the fuel with the ablator; dropping its areal density (ρr) and causing inefficient burn of the fuel. It is important, therefore, to minimize both the growth of RT instabilities and the size of their initial seeds.

Beryllium has been chosen as a preferred ablator material for x-ray-driven ignition experiments on the NIF for a number of reasons[5, 6], an important one being that its high density and high mass ablation rate makes it very tolerant to hydrodynamic instability growth. (RT growth is further reduced in the Be NIF point design capsule by the use of several sputtered Be layers, each with a slightly different amount of Cu doping to tailor

the density profile at the ablation front during the implosion)[7]. Additionally, Be is a very efficient ablator, with a low albedo, and thus offers the potential for successful ignition with much lower drive temperatures (~250eV), than other candidate materials such as plastic (CH). Its high tensile strength allows capsules to be filled with fuel at room temperature, and its high thermal conductivity helps in making the DT ice surface smooth in low modes.

However, Be is an anisotropic material with grains and other microstructure. It is possible that as the initial shock traverses across the ablator, the anisotropic response of the different grain orientations could cause pressure non-uniformities that will act as seeds for instability growth. The Be point design is designed to minimize this effect by ensuring that the first shock that passes through the Be has sufficient pressure to melt it. However, the outer surface of the capsule is also subjected to heating by radiation, both from the thermal environment of the hohlraum, and by higher energy m-band radiation produced by the interaction of the incident laser beams with the hohlraum walls. This radiation will penetrate some depth into the ablator and can potentially melt, or partially melt, the Be ahead of the shock front. Since the sound speed of solid Be is higher than that of liquid Be and the speed of sound in solid Be is actually different between crystal orientations, the coexistence of liquid and solid Be has the capacity to induce spatial perturbations in the first shock. Accurate measurements of the amount of Be material in the preheated coexistence regime can help to quantify the amount of shock front perturbation imposed in the NIF capsule due to partial melting of the Be.

It is important therefore to know how much of the Be ablator will be melted by thermal x-rays, and to verify whether the first shock will be sufficient to induce melt. Details of the radiation spectrum in the hohlraum are difficult to calculate, particularly the high energy m-band component[8]. It is therefore important to quantify the response of the ablator material under conditions as close to the actual ignition environment as possible.

To address the issue of material preheat prior to the arrival of the first shock in the beryllium we have carried out a series of experiments using the OMEGA laser system[9] at the University of Rochester to quantify conditions inside the outer 100 -120 μm of the ablator up to the arrival of the first shock. The experiments indicate the first 20 μm of the ablator will be melted by x-ray preheat. At greater depths the Be will be melted by the passage of the first shock. Absorption by the Cu-doped beryllium induces no measurable thermal expansion of the Be prior to shock break out indicating that the ignition design is robust to the presence of the higher energy components produced by laser energy absorption at the hohlraum wall.

Experiment

The experiment was designed to approximate conditions in the first few nanoseconds of the NIF foot pulse for the pole of the ignition capsule. We believe the two key criteria that must be met to assure surrogacy of the drive environment are: matching the radiation drive temperature (T_r) next to the ablator material; and matching the amount of Au m-

band radiation sampled by the pole. Of the two, the m-band radiation is the hardest to match. We do so by using a shortened half hohlraum, or halfraum and by placing the to-be-measured samples over the end opposite the laser entrance hole (LEH). The Omega laser beams are aimed at the inner-radius walls of the halfraum with power history and spot sizes chosen to closely match the expected conditions of the outer beams in the NIF ignition hohlraum. We purposely ignore the inner cone beams striking the middle of the NIF hohlraum when calculating the conditions for the pole of the capsule since their scattered radiation does not have a direct view of the pole.

The amount of Au m-band radiation present will depend on the intensity of the laser spots and the surface area of the wall illuminated. The equivalent wall fraction illuminated by the outer beams in the NIF hohlraum is ~21%. The NIF expected laser intensity at the wall, taking into account the energy reduction caused by gas burn-through, is ~2.3 x 10^{13} W/cm^2. The lower energy limits of the Omega laser facility in comparison to the NIF require the use of a smaller, scaled hohlraum in order to match the radiation drive temperature. We chose a halfraum with a diameter of 2.7 mm, length of 2.0 mm, and a laser entrance hole (LEH) of 60% (1.6 mm, see figure 1). We oriented the LEH to face the Omega H7 axis[10] and used a subset of the 21 available beams. For such a configuration the beams are divided into 22° (cone 1, 6 available beams), 48° (cone 2, 6 available beams), and 60° (cone 3, 12 available beams) cones. To avoid beam overlap (and best match the illuminated wall fraction) we chose to use all of the cone 2 beams with SG4 distributed phase plates [1112] focused at the LEH and three of the cone 3 beams with 200 x 300 micron phase plates defocused by -2 mm from the LEH plane. Cone 1

beams could be brought in at the end of the Cone 2/Cone 3 beams to maintain T_r while the shock propagated through the thicker material samples. Cone 1 beams were aimed at the wall opposite the LEH so that the Au wall shielded the sample from m-band production due to Cone 1 beam spots.

A "reverse ramp" pulse shape of three nanoseconds in duration was chosen for all beams. This pulse maintained the required radiative drive condition in the hohlraum until shock breakout was measured at the back of the sample (using the delayed cone 1 beams,if necessary). The energy per beam was chosen to achieve surrogacy at the Au wall. Omega laser intensity at the Au wall for the Cone 2 and Cone 3 beams is 2.2×10^{13} W/cm^2 in comparison to 2.3×10^{13} W/cm^2 for NIF. The reverse ramp pulse produced a relatively flat radiation temperature of ~83 eV which compares favorably with the predicted NIF radiation temperature of 84 eV. The equivalent illuminated wall area for Omega is ~18% which is somewhat lower than the ~21% expected on the NIF.

One proposed NIF ignition design consists of a Be capsule with an outer 100 μm layer of pure Be with interior layers of Be doped with ~0.35% to ~0.7% Cu [7].

The experiments described in this paper were designed to investigate conditions in both the outer Be layer and the first Cu-doped Be layer in such a capsule as the first shock passes through. Planar samples were attached to a 750-900 μm dia. diagnostic hole opposite the LEH. To investigate conditions in the outer part of the ablator, the samples consisted of a series of planar stepped foils of pure Be, with the smooth side pointing towards the radiation drive. The step thicknesses ranged from ~19 μm to ~51 μm. A subsequent set of experiments used a full thickness of Be, with a series of Cu-doped steps.

The experiments were simulated using the radiation hydrodynamics code Lasnex[13]. The shots with the thicker Be samples could be simulated by an integrated 2D Lasnex simulation that included the lasers, the Au hohlraum walls, and the planar sample on the back wall. To improve the resolution in the shots with the thinner Be samples, we used 1D simulations driven by a frequency dependent source (*fds*). The *fds* is created from the 2D simulations and is taken from a running time average of the multigroup power spectra over the central region of the hohlraum. The central region of the hohlraum, due to the near-isentropic nature of the interior hohlraum environment away from the laser spots, is a good approximation to the drive conditions on the sample for laser pulses only a few nanoseconds in duration. Thus, the *fds* contains the power history of the hohlraum energy that drives ablation in the sample. Electron temperature, opacities, velocities, and densities were saved at set time intervals and used to produce simulated data for comparison to the experimentally measured data.

Instruments

The temperature inside the OMEGA halfraum was measured using the multichannel x-ray diode array, Dante [14] .The measured radiation temperature for one of the thicker Be cases is shown in figure 2, together with the Lasnex calculated T_r drive for that shot. Motion of the rear surface of the Be samples was measured using a two-channel line VISAR system [15], which can measure velocity as a function of time by detecting the Doppler shift of light reflecting from the surface. Laser light reflected from the target is imaged through an interferometer onto the slit of an optical streak camera. The resulting image contains a series of fringes, with phase directly proportional to the velocity of the

reflecting surface. For the pure Be experiments described in this paper a pair of interferometer/streak camera channels was used with sensitivities of 0.859 km s^{-1} $fringe^{-1}$ and 0.645 km s^{-1} $fringe^{-1}$. With detection threshold of 1/20 fringe, the minimum detectable motion of the rear surface would be ~40 m s^{-1}. In addition to temporal information the diagnostic can give one-dimensional spatial information.

Results and Analysis

Figure 3 shows data and the measured rear surface motion from a pure Be stepped foil driven by the 3.0 ns drive. In this case the steps were 19.4, 36.1, and 50.6 μm. Fringe motion from the thinnest step, corresponding to surface acceleration can be seen very soon after the start of the drive, reaching a speed of 800 m/sec at 1 ns. The thicker steps also start to move, but at progressively later times, as the amount of preheat is reduced by the increased areal density. The signal from the thicker steps ends abruptly at ~2 and ~3 ns respectively. The sudden cut-off in reflectivity at that time is caused by the breakout of the Mbar-level shock generated by the radiation drive, which causes the material to unload. (The step in the cut-off is due to the interferometer used in the VISAR. The non-delayed arm of the interferometer loses signal first, causing a loss of fringe contrast. The signal from the second arm falls to zero after a time equal to the delay time of the interferometer.) The thinnest step shows a less sharp drop-off in signal. In this case it is possible that the Be surface may begin to unload due to preheat at the same time or just before the arrival of the shock.

Figure 4 shows a comparison between the measured and calculated rear surface velocities for a range of Be step thicknesses, from 19.4 to 51 μm. The experimental data was derived from two different shots with identical drive conditions. The simulations reproduce well the observed preheat velocities and shock breakout times for each foil thickness, indicating that the model provides a good match to both the temperature and shock strength in the foil. The predicted rear-surface temperatures of the Be foil samples are shown in fig 5. The melting point of unshocked Be is 0.134 eV, which is reached by the 19.4 μm sample after ~1.1 ns, before the shock arrival time. It is possible to use the simulations to look at conditions inside the beryllium sample as a function of time. Figure 6 shows the temperature calculated by Lasnex inside the beryllium as a function of distance at several times during the drive. Also plotted is the predicted Be melt line as a function of distance at the same times. The melt temperature is significantly higher in the compressed material behind the shock– the sudden increase corresponds to the position of the shock front. However, the temperature rise created by the ~3.5 Mbar shock is more than a factor of two times that required to melt the foil.

At early times the temperature profiles show there is a sufficient amount of radiative preheat to melt the Be in front of the shock. For example, at 1.0 ns, it is predicted that the foil will be melted about 7 μm ahead of the shock (about 200-300 ps before shock arrival) However, at greater distances into the foil the temperature induced by the radiation is much less, and melting is caused by passage of the shock (e.g. see the curves at 1.8 ns). The distance inside the foil at which the transition between x-ray melting and shock melting occurs is about 22 μm – just slightly more than the thinnest foil used in the Omega experiment.

Energy deposition into the material is expected to decay exponentially with depth which means that the majority of the shell is melted by the shock. The lower temperature of the ablator near the DT ice interface helps to avoid the seeding of high mode surface roughness via thermal expansion of the Be ablator. The thermal expansion is an issue since the expansion of Be is asymmetric along crystal planes and the deposited Be ablator is crystalline.

Although the pure Be shots indicate that any temperature rise due to preheat is negligible at several tens of microns into the ablator, it is possible that Au m-band radiation could penetrate through the 105 μm Be layer and preferentially deposit in the Cu-doped layer underneath it. This potential effect was studied using stepped foils consisting of ~105 μm pure Be backed with 10 μm and 20μm steps of 0.35% Cu-doped Be as shown in figure 7. The VISAR used during this series had a channel with a maximum sensitivity of 0.829 km s^{-1} $fringe^{-1}$. The measured VISAR traces for the first two steps are shown in figure 8. There is no discernable motion of the rear surface for either the pure Be sample or the sample with the 10 μm Cu-doped layer, in agreement with the simulations. The lack of motion from the doped sample indicates that the temperature in the doped region must be significantly below the melt temperature. Thermal expansion driven by m-band energy deposited at the front of the doped layer during the 3 ns laser drive would have plenty of time to travel through the 10 μm doped layer at the sound speed (13 um/ns is elastic sound speed of solid Be) & cause motion before shock breakout. Fig 8 also shows a trace from a foil with a thicker (20 μm Cu-doped layer) In this case we used 6 of the 60^0 beams to increase the m-band fraction even higher, but again saw no detectable motion at the rear surface

Summary

We have carried out a series of experiments designed to investigate conditions inside a candidate ablator material during the first few ns of the ignition drive of the NIF. Using a scaled halfraum on the OMEGA laser system we were able to match the NIF radiation drive, the illuminated wall fraction and the laser intensity at the halfraum wall. Thin Be samples, designed to probe conditions inside the first few tens of microns inside the ablator, show evidence of the expected radiative preheating ahead of the initial shock front. The experimental data are well reproduced by integrated simulations of the conditions inside the hohlraum. The simulations and experiment show that the ablator will be melted by radiation to a depth of 20-25 μm, after which the Be remains solid until melted by passage of the shock. Experiments using "full thickness" pure Be layers with a buried Cu-doped layer also show that there is no measurable heating of the buried layer. These results are important because they indicate that radiative preheat will not play a role in seeding instabilities at the DT ice/Be interface and that the melting of the outer surface of the pure Be layer is in agreement with simulations.

This work was performed under the auspices of the U.S. Department of Energy by Lawrence Livermore National Laboratory in part under Contract W-7405-Eng-48 and in part under Contract DE-AC52-07NA27344.

Figure Captions

Figure 1. Schematic showing the halfraum used in these experiments. The stepped foil is shown not to scale.

Figure 2. Comparison of the measured (solid line), and simulated (dotted) T_r as a function of time

Figure 3. (a) Raw VISAR image recorded from stepped pure Be foil and (b) corresponding velocity histories measured from the 3 steps

Figure 4. Measured (dotted) and predicted (solid) foil surface velocities for a range of initial step thicknesses. From left: 19.4 μm, 31 μm, 36 μm, 46 μm, and 51μm

Figure 5. Predicted rear-surface temperatures corresponding to the samples shown in figure 4.

Figure 6. Simulated temperature profiles and melt lines as a function of distance into the Be sample at 200 ps increments during the laser pulse. (a) during the first ns of the pulse, melting occurs due to radiation, (b) between 22 and 28 μm melting starts to occur due to shock heating

Figure 7. Schematic of the stepped sample used to measure energy deposition in buried Cu-doped layers

Figure 8. Measured and simulated surface motion from the thick Be samples and the 0.35%Cu-doped steps. The vertical lines denote shock breakout. From left to right the curves are 107 um pure Be(~84 eV drive), 108umBe + 10umBeCu(~88 eV drive), 107umBe+10umBeCu(~84 eV drive), 107umBe + 30umBeCu(~88eV drive). The ~88 eV drive shots were with an increased m-band (6 cone 3 beams were used with each beam having some overlap with the Cone 2 spots).

References

[1] J. D. Lindl, P. Amendt, R. L. Berger, et al., Physics of Plasmas **11**, 339 (2004).

[2] J. A. Paisner, J. D. Boyes, S. A. Kumpan, et al., Laser Focus World **30**, 75 (1994).

[3] S. Chandrasekhar, *Hydrodynamic and Hydromagnetic Stability* (Oxford University Press, London, 1968).

[4] G. Taylor, Proceedings of the Royal Society of London, Series A (Mathematical and Physical Sciences) **201**, 192 (1950).

[5] S. W. Haan, P. A. Amendt, R. T. Dittrich, et al., Fusion Science and Technology **45**, 69 (2004).

[6] S. W. Haan, P. A. Amendt, T. R. Dittrich, et al., Nuclear Fusion **44**, S171 (2004).

[7] S. W. Haan, M. C. Herrmann, T. R. Dittrich, et al., Physics of Plasmas **12**, 56316 (2005).

[8] P. A. Amendt, H. F. Robey, H. S. Park, et al., Physical Review Letters **94**, 065004/1 (2005).

[9] T. R. Boehly, D. L. Brown, R. S. Craxton, et al., Optics Communications **133**, 495 (1997).

[10] National Laser Users' Facility Users' Guide http://www.lle.rochester.edu/pub/documents/ext/nluf_users_guide.pdf

[11] Y. Lin, T. J. Kessler, and G. N. Lawrence, Optics Letters **20**, 764 (1995).

[12] The SG4 phase plates are distributed phase plates (DPP's) with a super-Gaussian focal spot profile at best focus with order n=5, and a 1/e radius of 350 (m

[13] G. B. Zimmerman and W. L. Kruer, Comments on Plasma Physics and Controlled Fusion **2**, 51 (1975).

[14] H. N. Kornblum, R. L. Kauffman, and J. A. Smith, Review of Scientific Instruments **57**, 2179 (1986).

[15] P. M. Celliers, D. K. Bradley, G. W. Collins, et al., Review of Scientific Instruments **75**, 4916 (2004).

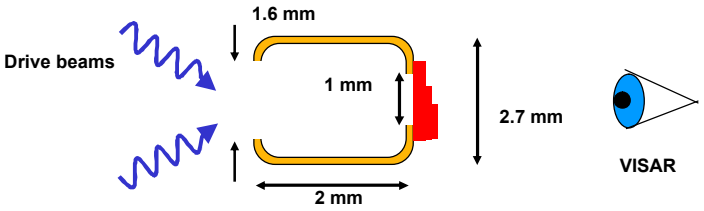

Figure 1

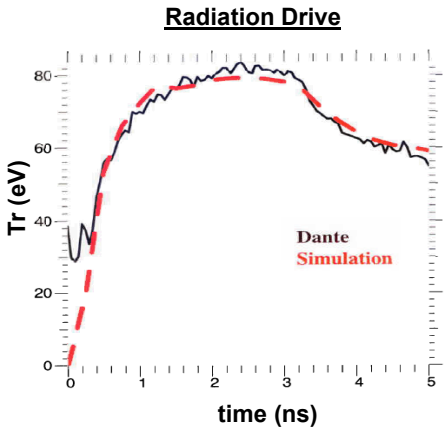

Figure 2

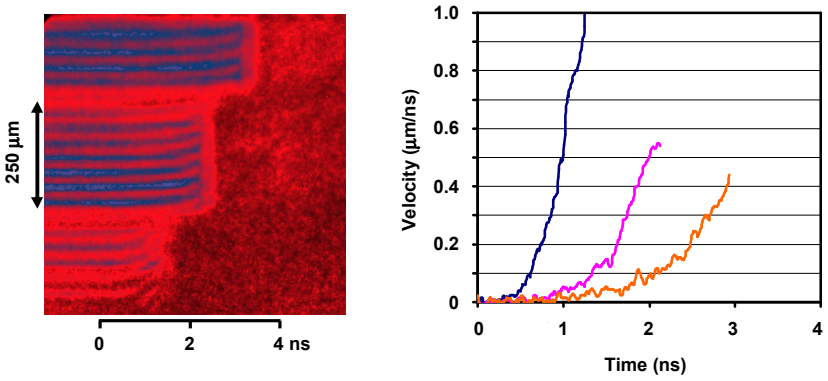

Figure 3

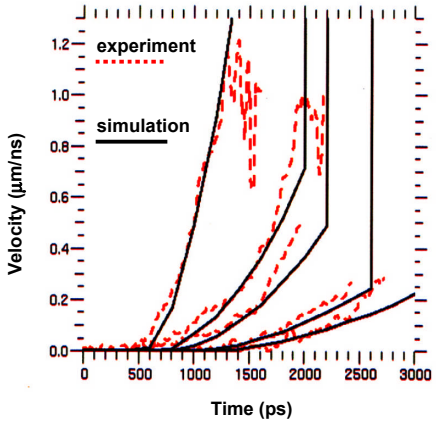

Figure 4

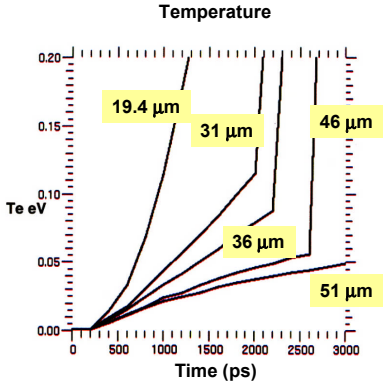

Figure 5

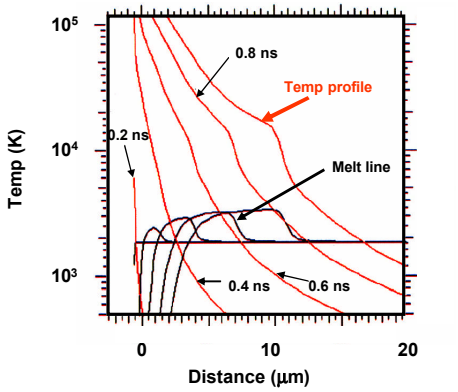

Figure 6 (a)

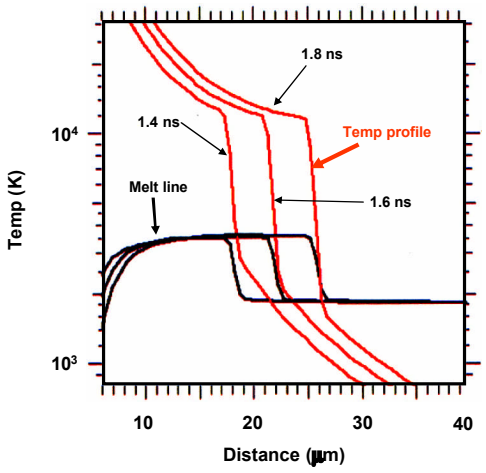

Figure 6 (b)

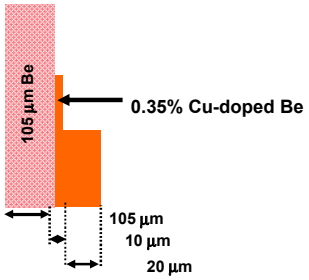

Figure 7

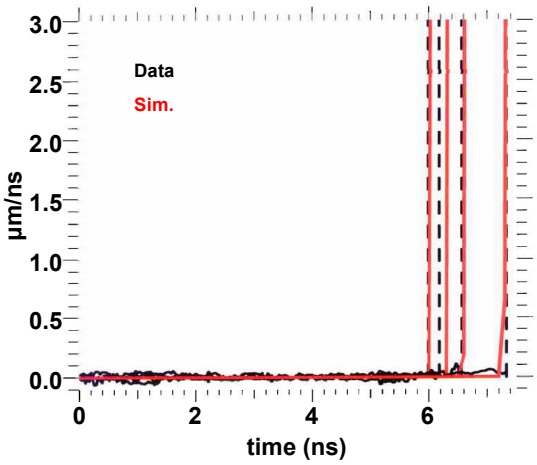

Figure 8